THE JOURNAL OF PHYSICAL CHEMISTRY Letters

Letter

pubs.acs.org/JPCL

# Unusual Activity Trend for CO Oxidation on $Pd_xAu_{140-x}$@Pt Core@Shell Nanoparticle Electrocatalysts

Long Luo,[†,∥] Liang Zhang,[†,§,∥] Graeme Henkelman,*[,†,§] and Richard M. Crooks*[,†,‡]

[†]Department of Chemistry, [‡]Texas Materials Institute, and [§]Institute for Computational and Engineering Sciences, The University of Texas at Austin, 105 East 24th Street, Stop A5300, Austin, Texas 78712-1224, United States

Supporting Information

**ABSTRACT:** A theoretical and experimental study of the electrocatalytic oxidation of CO on $Pd_xAu_{140-x}$@Pt dendrimer-encapsulated nanoparticle (DEN) catalysts is presented. These nanoparticles are comprised of a core having an average of 140 atoms and a Pt monolayer shell. The CO oxidation activity trend exhibits an unusual koppa shape as the number of Pd atoms in the core is varied from 0 to 140. Calculations based on density functional theory suggest that the koppa-shaped trend is driven primarily by structural changes that affect the CO binding energy on the surface. Specifically, a pure Au core leads to deformation of the Pt shell and a compression of the Pt lattice. In contrast, Pd, from the pure Pd cores, tends to segregate on the DEN surface, forming an inverted configuration having Pt within the core and Pd in the shell. With a small addition of Au, however, the alloy PdAu cores stabilize the core@shell structures by preventing Au and Pd from escaping to the particle surface.

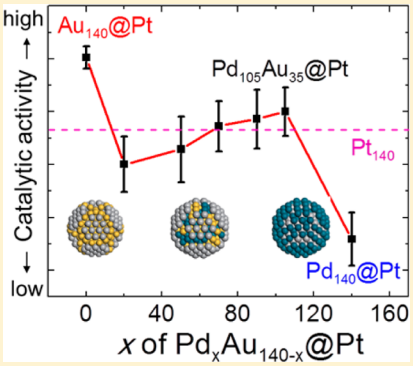


Here we report the synthesis and characterization of $Pd_xAu_{140-x}$@Pt core@shell dendrimer-encapsulated nanoparticles (DENs), and discuss their unusual electrocatalytic activity toward adsorbed CO oxidation as a function of the core composition. Specifically, as $x$ in $Pd_xAu_{140-x}$@Pt is varied from 0 to 140, a "koppa (ϰ)-shaped" electrocatalytic activity trend is observed. In other words, the catalytic activity profile exhibits two rapid decreases at low and high values of $x$, and a slow increase at intermediate values. This result is different from the more common linear- or volcano-shaped variation in activity.[1−7] Other unusual catalytic trends have been reported for bimetallic nanoparticles, but these are nearly always caused by electronic effects.[8,9] In contrast, density functional theory (DFT) suggests that the koppa-shaped trend observed in our system is caused primarily by structural changes at high and low values of $x$. This in turn leads to a change in the CO binding energy on the surface.

$Pd_xAu_{140-x}$@Pt core@shell DENs were synthesized using a previously reported three-step procedure (Scheme 1):[3,10−12] (1) formation of the $Pd_xAu_{140-x}$ core, (2) underpotential deposition (UPD) of a Cu shell onto the core, and (3) galvanic exchange of Pt for the Cu shell. More specifically, in the first step, $x$ equivalents of $K_2PdCl_4$ were added to a 2.0 $\mu$M aqueous solution of sixth-generation, hydroxyl-terminated poly(amidoamine) dendrimer (G6-OH). The appropriate number of equivalents of $Pd^{2+}$ were then allowed to complex with G6-OH for 15 min in a $N_2$-purged aqueous solution. Next, $140 - x$ equivalents of $HAuCl_4$ were added to the solution, followed by addition of a 10-fold excess of $NaBH_4$ (in 0.30 M NaOH) within 2 min. This results in reduction of the G6-OH-$(Pd^{2+})_x(Au^{3+})_{140-x}$ precursor to the G6-OH($Pd_xAu_{140-x}$) DEN core. This DEN core was then immobilized on Vulcan EC-72R carbon by sonicating in a solution containing the DENs (2.0 $\mu$M) and Vulcan (1.0 mg per 1.0 mL solution) for 5 min under $N_2$. A small volume (10.0 $\mu$L) of the resulting ink was drop cast onto a freshly polished glassy carbon electrode (GCE) and then the electrode was dried under mild Ar flow. In Step 2, the Cu shell was added to the $Pd_xAu_{140-x}$ core by UPD of a monolayer of Cu from a 10.0 mL solution containing 5.0 mM $CuSO_4$ and 0.10 M $HClO_4$. Finally, in Step 3, the Cu UPD shell was exchanged for Pt by injecting 100.0 $\mu$L of a solution containing 10.0 mg of $K_2PtCl_4$ dissolved in deaerated 0.1 M $HClO_4$ into the Cu deposition solution. The final product, $Pd_xAu_{140-x}$@Pt, and the two intermediates, $Pd_xAu_{140-x}$ and $Pd_xAu_{140-x}$@Cu, were characterized by transmission electron microscopy (TEM), electrochemical methods, and DFT.

Figure 1a shows cyclic voltammograms (CVs) of $Pd_{140}$ and $Au_{140}$ single-element DENs obtained in 0.10 M $HClO_4$. The current densities were calculated using surface areas determined by Cu UPD experiments.[13,14] The $Pd_{140}$ DENs exhibit a Pd oxidation current positive of ∼0.1 V, a corresponding $PdO_x$ reduction peak centered at ca. −0.2 V, and a pair of current excursions corresponding to hydride formation and subsequent oxidation near the negative potential scan limits. By contrast, the CV obtained using the $Au_{140}$ DEN-modified electrode is featureless except for the characteristic background capacitance. The CVs of the PdAu alloy−core DENs (Figure 1b and S1) reveal features intermediate between the $Au_{140}$ and $Pd_{140}$ DENs. This trend shows a smooth transition toward the

**Received:** May 12, 2015
**Accepted:** June 15, 2015





DOI: 10.1021/acs.jpclett.5b00985
J. Phys. Chem. Lett. 2015, 6, 2562−2568

**Scheme 1**

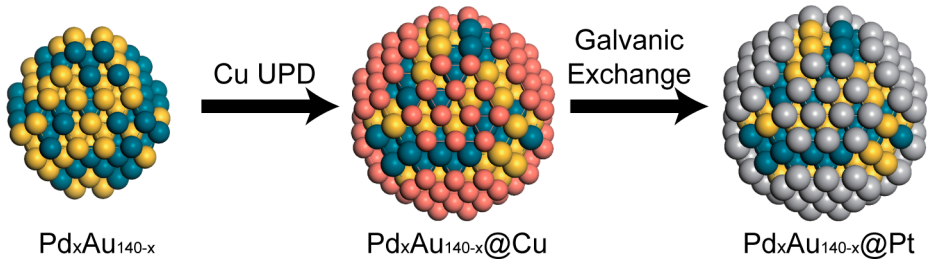


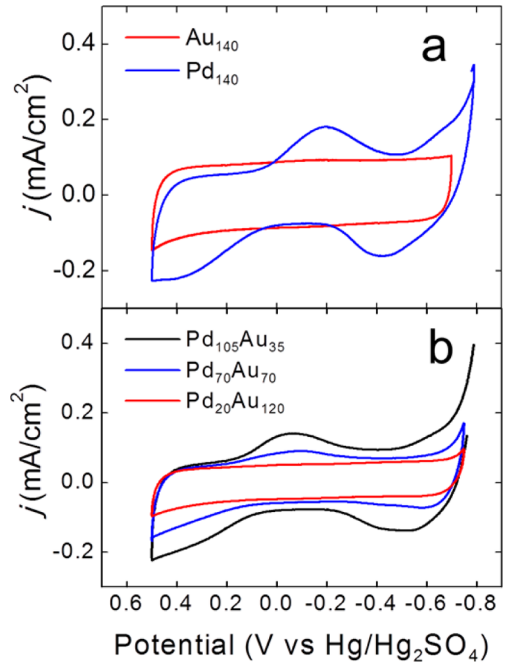


**Figure 1.** CVs of $Pd_xAu_{140-x}$ DENs supported on Vulcan carbon. The CVs were obtained using a glassy carbon working electrode, a $N_2$-purged 0.10 M $HClO_4$ aqueous electrolyte solution, and a scan rate of 100 mV/s.

appearance of the $Pd_{140}$ CV as the mole fraction of Pd increases. Trends similar to those observed for DEN-modified electrodes have also been reported by Maroun et al. for macroscopic PdAu alloy electrodes.[15] This agreement of the trends in CVs suggests a random alloy configuration of this group of alloy DENs, which is also consistent with our previous studies using extended X-ray absorption fine structure (EXAFS) spectroscopy.[16,17]

$Pd_xAu_{140-x}$@Cu DENs were prepared by UPD of a monolayer of Cu on a $Pd_xAu_{140-x}$ core, and then they were studied by voltammetry. Cu electrodeposition was carried out by holding the potential of the $Pd_xAu_{140-x}$ DEN-modified electrode at −0.40 V (slightly positive of the bulk Cu deposition potential) for 100 s.[3,11] Next, the potential was slowly swept from −0.40 to 0.15 V to strip off the Cu monolayer in the same solution. Figure 2a shows the corresponding stripping voltammograms for $Pd_xAu_{140-x}$@Cu DENs ($x$ = 0, 20, 70, 90, 105 and 140). The anodic peaks between −0.40 to −0.10 V correspond to the oxidation of the Cu shell. In the absence of Cu UPD, no anodic peak was observed (Figure S2). More importantly, with increasing Pd content in the $Pd_xAu_{140-x}$ core, the stripping peaks shift negative from −0.20 V ($x$ = 0) to −0.32 V ($x$ = 140, Figure 2a).

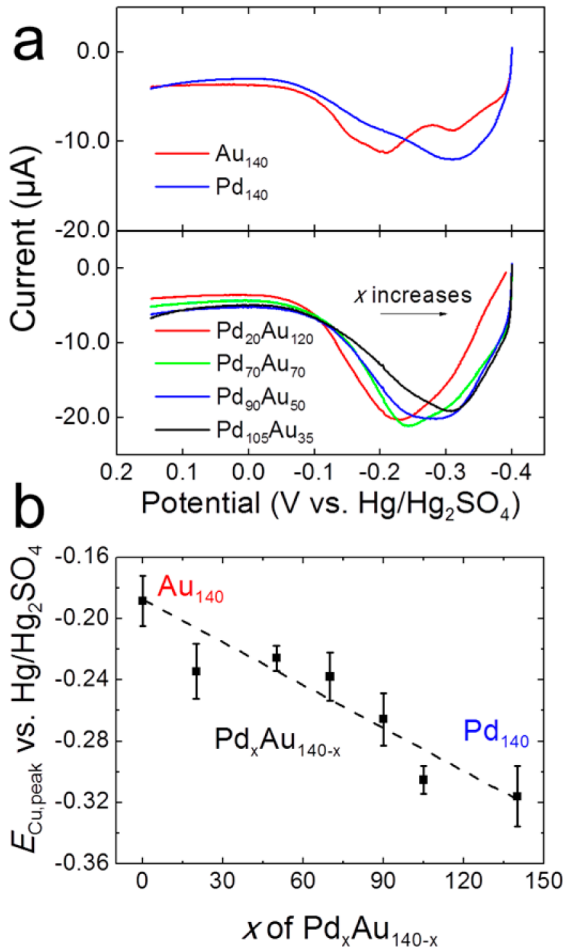


**Figure 2.** (a) Stripping voltammogram for $Pd_xAu_{140-x}$@Cu DENs. Upper panel: $Au_{140}$@Cu and $Pd_{140}$@Cu DENs, and lower panel: PdAu alloy@Cu DENs having the indicated core compositions. The Cu shell was deposited by holding the potential of the working electrode at −0.40 V for 100 s in 0.10 M $HClO_4$/5.0 mM $CuSO_4$. (b) Stripping peak position ($E_{Cu,peak}$) versus core composition ($x$ of $Pd_xAu_{140-x}$). The error bars are the standard deviations of at least three independent measurements. The scan rate for all CVs was 10.0 mV/s, and all solutions were degassed with $N_2$.

Figure 2b is a plot of the average (of at least three independent voltammograms) peak potential ($E_{Cu,peak}$) as a function of core composition ($x$ of $Pd_xAu_{140-x}$). It reveals a linear trend having a slope of −1.1 mV/Pd atom. Consistent with the synthetic method used to prepare the cores, this result also suggests that the ratios of Pd and Au vary linearly. In other words, the Cu UPD process does not alter the composition or surface properties of the cores.



DOI: 10.1021/acs.jpclett.5b00985
J. Phys. Chem. Lett. 2015, 6, 2562−2568

The $Pd_xAu_{140-x}$@Pt DENs were synthesized by galvanic exchange of Pt for the Cu monolayer on the $Pd_xAu_{140-x}$@Cu DENs. During galvanic exchange, the open circuit potential (OCP) of the $Pd_xAu_{140-x}$@Cu DEN-modified electrode was recorded.[10,18,19] Figure 3a illustrates how the OCP changes for a particular core composition ($Pd_{105}Au_{35}$) when the $K_2PtCl_4$ solution is introduced. Before galvanic exchange ($t$ = 0), the OCP of the working electrode is ca. −0.4 V. Initially, there is a slight increase in the OCP due to slow oxidation of the Cu shell by trace $O_2$ present in the solution. Upon introducing $K_2PtCl_4$ at $t$ = 17 s, however, there is a rapid increase in the OCP until it reaches a limiting value ($V_{l,OCP}$) of 0.12−0.16 V. The stable final value of $V_{l,OCP}$ indicates that galvanic exchange is complete. All the DENs exhibited a similar value of $V_{l,OCP}$ (0.13 ± 0.01 V, Table S1) except for the $Au_{140}$@Pt DENs ($V_{l,OCP}$ = 0.16 ± 0.01 V). The similarity in the values of $V_{l,OCP}$ suggests that the structure of the Pt shell that forms on all the $Pd_xAu_{140-x}$ cores following galvanic exchange is identical or nearly so.

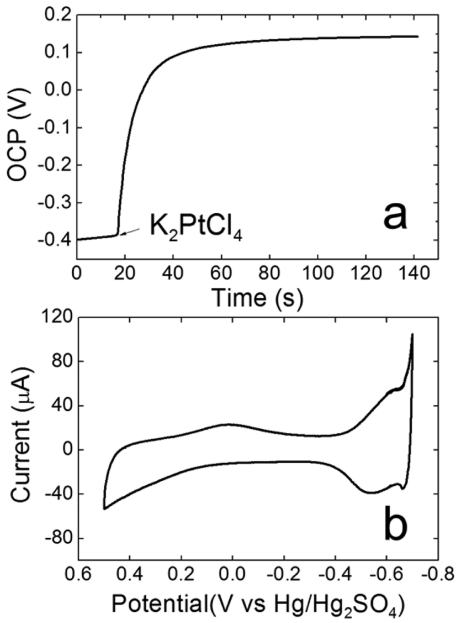


**Figure 3.** (a) A typical OCP versus time trace during galvanic exchange of Pt for the Cu shell on $Pd_{105}Au_{35}$@Cu DENs. (b) CV of the resulting $Pd_{105}Au_{35}$@Pt DENs (supported on Vulcan carbon) obtained using a glassy carbon working electrode, a $N_2$-purged 0.10 M $HClO_4$ aqueous electrolyte solution, and a scan rate of 100 mV/s.

A typical CV, obtained using 0.10 M $HClO_4$ as the electrolyte solution, of the $Pd_{105}Au_{35}$@Pt DENs that result from galvanic exchange is shown in Figure 3b. It shows the emergence of well-defined and stable H adsorption/desorption waves between −0.4 and −0.65 V and Pt oxidation ($E$ > 0.1 V) and subsequent reduction (peak potential = 0.0 V) waves, confirming the successful deposition of Pt on the $Pd_xAu_{140-x}$ DEN cores. The amount of Pt on the $Pd_xAu_{140-x}$@Pt DENs can be estimated from the H adsorption waves in these types of CVs (CVs for other core compositions are provided in Supporting Information Figure S1). The resulting values are nearly equal to the amount of Cu on the $Pd_xAu_{140-x}$@Cu DENs (calculated from the Cu stripping voltammetry, Figure S3), which correlates to complete replacement of Cu by Pt.

TEM was used to perform size analysis of the $Pd_xAu_{140-x}$ DENs (Figure 4a−c: $Au_{140}$, $Pd_{105}Au_{35}$, and $Pd_{140}$, respectively) and $Pd_xAu_{140-x}$@Pt DENs (Figure 4d−f: $Au_{140}$@Pt, $Pd_{105}Au_{35}$@Pt, and $Pd_{140}$@Pt, respectively). TEM micrographs for the other core compositions can be found in Figures S4 and S5. The TEM data indicate that the $Pd_xAu_{140-x}$ core DENs have a diameter of 1.6 ± 0.3 nm (Figure 4g−i), consistent with a calculated estimate (1.6 nm) and previous reports.[3,16,17] After the deposition of a Pt shell, the average size increases by ~0.6−

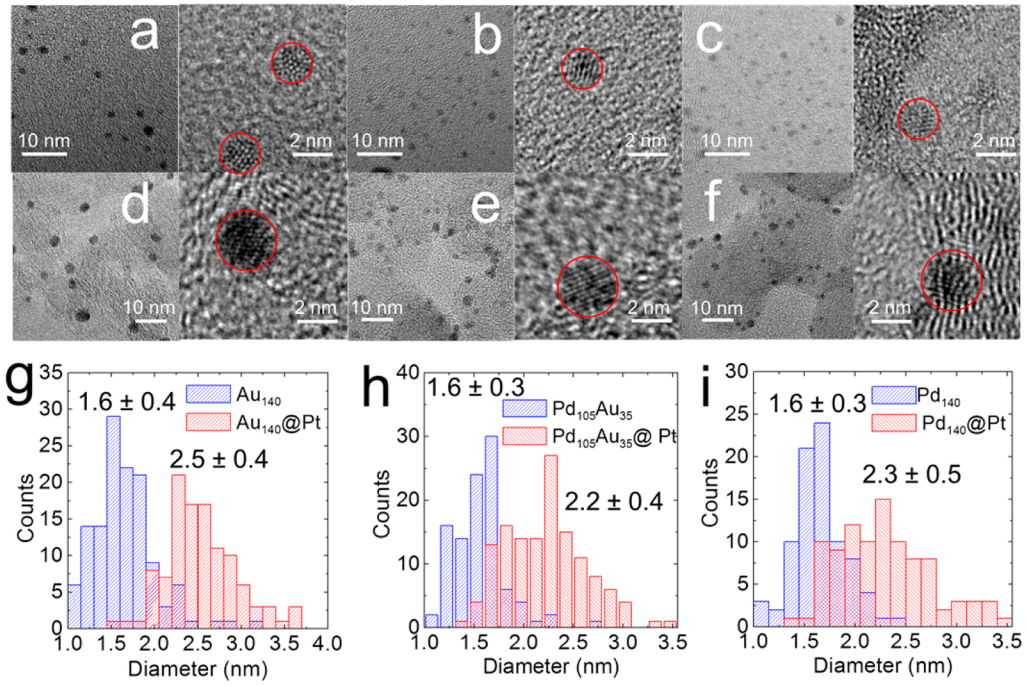


**Figure 4.** TEM micrographs of (a) $Au_{140}$, (b) $Pd_{105}Au_{35}$, and (c) $Pd_{140}$ core DENs and (d−f) the corresponding micrographs after addition of a Pt shell. The size distributions (g−h) were obtained by measuring at least 100 randomly selected DENs.



DOI: 10.1021/acs.jpclett.5b00985
J. Phys. Chem. Lett. 2015, 6, 2562−2568

0.9 nm, just slightly larger than the calculated ~0.5 nm increase.[20]

CO stripping voltammetry is the electrochemical method most commonly used to evaluate electrocatalysts for oxidation of surface-adsorbed CO ($CO_{ads}$).[12,21−30] For our experiments, a monolayer of CO on $Pd_xAu_{140-x}$@Pt DENs was formed by holding the DEN-modified electrode at $E$ = −0.60 V for 2.0 min in a CO-saturated 0.10 M $HClO_4$ solution. Next, $N_2$ was bubbled into the solution to displace dissolved CO while maintaining the electrode potential at −0.60 V. Finally, the potential was scanned positive to 0.50 V and negative to −0.65 V for three consecutive cycles. CO stripping voltammograms for all compositions of $Pd_xAu_{140-x}$@Pt DENs are provided in Figure S6, and an example (for $Pd_{105}Au_{35}$@Pt DENs) is shown in Figure 5a. During the first cycle (red) the H oxidation peak is absent (because the surface of the DENs are passivated with CO), but there is a large anodic peak between 0.10 and 0.40 V that is attributable to oxidation of adsorbed CO. In the second (black) and subsequent cycles, the CO oxidation peak is absent, but the typical waves associated with a Pt surface are all present. In all cases (Figure S7) CVs of $Pd_xAu_{140-x}$@Pt DENs in 0.10 M $HClO_4$ prior to and after CO oxidation experiments overlap, indicating no significant structural changes or size growth during CO adsorption or oxidation.

Expansions of the oxidation peaks for adsorbed CO on $Pd_xAu_{140-x}$@Pt ($x$ = 0, 20, 90, 105, and 140) DENs are shown in Figure 5b. Here, the currents are normalized to the Pt surface areas calculated from the H adsorption waves in the absence of CO. The charge associated with the CO oxidation peaks is about twice that of the corresponding H adsorption wave areas (Figure S8), suggesting nearly monolayer coverage of CO on Pt (recall CO oxidation is a two-electron process). In terms of peak potential ($E_{CO,peak}$), the catalytic activity of the $Pd_xAu_{140-x}$@Pt DENs has the following order in $x$: 140 < 20, 90, 105 < 0. More specifically, various alloy core@shell DENs exhibit a similar $E_{CO,peak}$ of ~0.2 V as the $Pt_{140}$ DENs, which is ~100 mV negative than $Pd_{140}$@Pt DENs but ~80 mV more positive than $Au_{140}$@Pt DENs. When plotted against the core composition ($x$ in $Pd_xAu_{140-x}$@Pt), the catalytic activity trend in terms of $E_{CO,peak}$ becomes koppa-shaped (Figure 5c). A similar trend, but with a larger standard deviation, is observed for the onset potentials for $CO_{ads}$ oxidation (Figure S9).

This koppa-trend can be interpreted by understanding the two turning points at low and high values of $x$, that is, $Au_{140}$@Pt and $Pd_{140}$@Pt, respectively. As previously reported by our group,[12] Au@Pt core@shell DENs exhibit a higher catalytic activity toward adsorbed CO oxidation than Pt DENs having a similar size. This is because the Pt shell of Au@Pt DENs undergoes a deformation corresponding to compressed Pt facets having an average Pt−Pt bond length shorter than in pure Pt DENs. Compression of the Pt−Pt bonds leads to weaker CO binding and improved catalytic activity for CO oxidation with respect to Pt DENs. For $Pd_{140}$@Pt DENs, the low activity is probably caused by inversion of the particles to yield a Pd shell that binds CO more strongly than Pt. Anderson et al. reported the spontaneous inversion of $Pd_{147}$@$Pt_{162}$ to $Pt_{147}$@$Pd_{147}Pt_{15}$ DENs where the corner and edge sites are considered to be the reactive sites for core−shell inversion.[31] A similar reconfiguration was observed for $Pd_{55}$@$Pt_{92}$[31] and $Pd_{55}$@$Au_{92}$ DENs.[17]

To test the aforementioned inversion hypothesis, $Pt_{140}$@Pd DENs were synthesized and the CO oxidation activity examined. The peak potential for CO oxidation on the

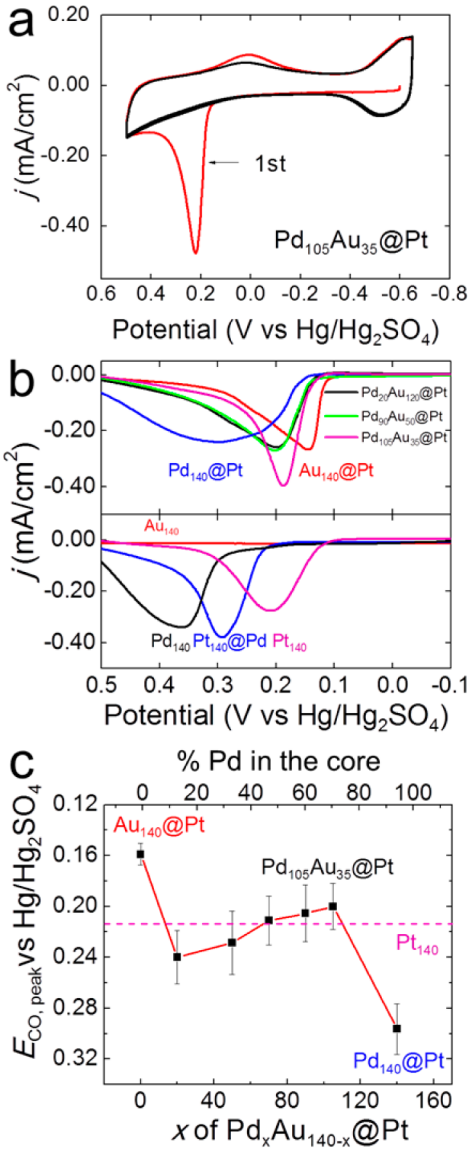


**Figure 5.** (a) CV showing the oxidation of $CO_{ads}$ on $Pd_{105}Au_{35}$@Pt DENs. The oxidation current is normalized to the Pt surface area, which is calculated from the H adsorption waves in Figure S1. The red line indicates the first cycle and the black line is the second cycle. (b)Upper panel: Peaks corresponding to oxidation of $CO_{ads}$ for $Pd_{140}$@Pt, $Pd_{20}Au_{120}$@Pt, $Pd_{90}Au_{50}$@Pt, $Pd_{105}Au_{35}$@Pt, and $Au_{140}$@Pt DENs. Lower panel: control experiments using $Au_{140}$, $Pd_{140}$, $Pt_{140}$@Pd and $Pt_{140}$ DENs. Complete CVs are provided in Figure S6. (c) CO stripping peak potential ($E_{CO,Peak}$) versus $x$ in $Pd_xAu_{140-x}$@Pt DENs exhibiting a koppa-like shape. Error bars represent the standard deviations of at least three independent tests. For panels a and b, the DENs were supported on Vulcan carbon and the CVs obtained using a glassy carbon working electrode and a $N_2$-purged 0.10 M $HClO_4$ aqueous electrolyte solution. The scan rate for all CVs was 50 mV/s.

$Pt_{140}$@Pd DENs (~0.3 V) is close to that observed for the $Pd_{140}$@Pt DENs (Figure 5b), suggesting that structural inversion is the likely cause of the lowered activity. In contrast to monometallic cores, the alloy cores tend to stabilize the core@shell structure. This conclusion is similar to that reported by Adzic and co-workers, wherein larger (~4 nm) PdAu alloy cores stabilized monolayer Pt shells. Indeed, they reported little structural degradation for the oxygen reduction reaction (ORR) even after 100 000 potential cycles.[32,33] They ascribed the



DOI: 10.1021/acs.jpclett.5b00985
J. Phys. Chem. Lett. 2015, 6, 2562−2568

stability improvement to the occupancy of low-coordinated surface defects by Au atoms. To summarize, we believe the koppa trend is caused by a combination of structural deformation with a pure Au or Pd core and structural stabilization by PdAu alloy cores.

DFT calculations were performed to further understand the experimentally observed catalytic activity trends described in the previous paragraph. Specifically, CO binding energies on $Pd_xAu_{140-x}@Pt_{96}$ particles ($x$ = 0, 35, 70, 105, and 140) were calculated to determine the oxidation potential of adsorbed CO. It is generally accepted that oxidation of CO adsorbed on Pt occurs primarily via a Langmuir−Hinshelwood (L−H) mechanism, which means adsorbed CO reacts with adsorbed oxygen-containing species.[34] Previous studies show that the binding energy of CO and OH are good descriptors for understanding CO electrooxidation activity.[4,35] In the case of alloy-core@shell nanoparticles, for example, Zhang et al. showed that there is often a linear correlation between the binding energy of adsorbates to the shell and the composition of the alloy core. This correlation is general across a range of nanoparticle compositions, sizes, and adsorbate molecules.[7] In fact, we found a similar positive correlation for CO and OH binding to the nanoparticles reported here (Figure S10). Based on these DFT calculations and the experimental data, we conclude that the change in oxidation potential is caused primarily by the difference in CO binding, and therefore only the binding of $CO_{ads}$ was used as a descriptor.

The nanoparticles were modeled as face-centered cubic (fcc) crystallites with a 140-atom truncated octahedral $Pd_xAu_{140-x}$ alloy core. The Pt shell was modeled with 96 atoms covering the (111) facets, leaving the corner and edge sites exposed (Scheme 1 and Figure 6a). We have evidence from previous experimental characterization of similar DENs that this model is reasonable.[11,13,14] The CO binding energy, $E_b$, was calculated as an average over the atop binding sites in the center of each of the eight (111) facets,

$$E_b = 1/8(E_{NP+8CO} - E_{NP} - 8E_{CO}) \quad (1)$$

Here, $E_{NP+8CO}$ is the energy of the particle with eight adsorbed CO molecules, $E_{NP}$ is the energy of the bare particle, and $E_{CO}$ is the reference energy of a free CO molecule. Ten different random-alloy configurations were considered in the calculation of the average CO binding energy for each core composition (80 binding sites, in total). Additional computational details can be found in the Supporting Information.

The solid line in Figure 6b shows that as $x$ is varied, the calculated CO binding energy correlates well with the experimental result shown in Figure 5c. By comparing the experimental results with the theoretical calculations, the $E_{CO,peak}$ was found to shift positive when CO and OH binding becomes stronger. This indicates that $CO_{ads}$ oxidation by $OH_{ads}$ determines the CO oxidation potential in our system. Otherwise, if the OH nucleation step determined the oxidation potential, $E_{CO,peak}$ would shift negative with stronger OH binding. The latter trend is not observed. In Region I (RI), where 25% Pd is alloyed to the Au core forming $Pd_{35}Au_{105}@Pt_{96}$, CO binding is enhanced by ~0.4 eV compared to $Au_{140}@Pt_{96}$, and the average Pt−Pt bond length increases from 2.65 to 2.70 Å (Figure S11). These observations are understood in terms of a deformation of the Pt shell on the $Au_{140}@Pt_{96}$ nanoparticles. The optimized structure of $Au_{140}@Pt_{96}$ in Figure 6a shows that atoms from the Au core protrude at the edges and corners, while the Pt shell facets are compressed by the

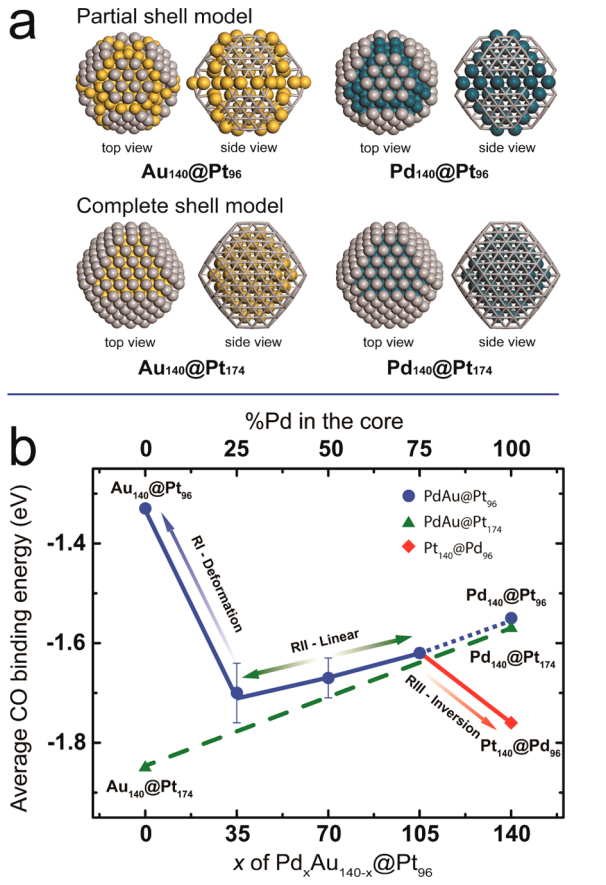


**Figure 6.** (a) DFT-optimized structure of the partial-shell and complete-shell models: $Au_{140}@Pt_{96}$, $Pd_{140}@Pt_{96}$, $Au_{140}@Pt_{174}$, and $Pd_{140}@Pt_{174}$. The gold, blue, and gray spheres represent Au, Pd, and Pt atoms, respectively. In side view figures, the Pt shells are shown as frames to highlight the structure deformation of $Au_{140}@Pt_{96}$ (that some Au core atoms are actually on the same plane as the Pt shell). (b) The calculated CO binding energy trend of PdAu@Pt nanoparticles as a function of percentage of Pd in the core for the models shown in (a).

surrounding Au atoms. Similar to our previous findings, the weak CO binding of $Au_{140}@Pt_{96}$ is a consequence of this deformation of Pt partial shell.[12] The addition of small amounts of Pd in the core, however, suppresses this effect and recovers the expected strong CO binding of a Pt overlayer on Au. This argument is further supported by consideration the complete shell model $Au_{140}@Pt_{174}$, where the significant Au deformation is suppressed. Clearly, $Au_{140}@Pt_{174}$ binds CO more strongly than either $Au_{140}@Pt_{96}$ or $Pd_{35}Au_{105}@Pt_{96}$ in the absence of such a deformation.

By increasing the Pd fraction in the alloy core of $PdAu@Pt_{96}$ from 25% to 75% (RII in Figure 6b), the CO binding is slowly and linearly weakened by 0.1 eV. A similar trend is observed for the complete shell model, $PdAu@Pt_{174}$, at the same Pd fractions (dashed line in Figure 6b). This trend can be explained by strain in the Pt shell due to the core alloy.[36,37] In our case, the Pt−Pt bonds are stretched with an increasing Au composition in the core. The calculated Pt−Pt bond length illustrates this trend (Figure S11). The slight discrepancy between the solid line and the dashed line is likely caused by minor shell deformations, especially at higher Au content.

Shell deformation and strain explain the trends in the RI and RII regions of Figure 5c. In RIII, where the majority of the core



DOI: 10.1021/acs.jpclett.5b00985
J. Phys. Chem. Lett. 2015, 6, 2562−2568

is Pd, we attribute the drop in activity to the inversion of Pd and Pt between the core and the shell. This explanation is supported by the fact that the CO stripping potential in the Pd-rich DENs is similar to that observed for $Pt_{140}$@Pd DENs (Figure 5b), in which Pd is known to be in the shell. In Figure 6b, DFT calculations show that CO binds more strongly to $Pt_{140}$@$Pd_{96}$ (−1.77 eV) than $Pd_{140}$@$Pt_{96}$ (−1.55 eV), giving rise to the second transition in the koppa-shaped plot of CO stripping potential (Figure 5c). Importantly, the addition of just a small amount of Au to the Pd core dramatically suppresses the inversion process. The segregation energy to swap a Pt atom in the shell with a subsurface Pd atom was calculated on $Pd_{140}$@$Pt_{96}$ to be −0.29 eV. With the addition of 25% Au, in the $Pd_{105}Au_{35}$@$Pt_{96}$ particle, this segregation energy is cut in half, demonstrating the increase in shell stability (Figure S11). The reduction of $E_{seg}$ indicates that alloying of Au makes the core bind Pd atoms more strongly than Pt, which is very likely due to the stronger interaction between Au−Pd compared to Au−Pt. Although $E_{seg}$ remains negative (thermodynamics favorable for segregation), it could still be kinetically stabilized. $E_{seg}$ provides a simple model to evaluate the stability, and we are more interested in the trend of $E_{seg}$ instead of its absolute value or its sign. This alloy stability is also supported by the positive curvature of the convex hull for PdAu random alloy formation, (Figure S12) demonstrating that alloying Au and Pd is energetically favorable as compared to the monometallic nanoparticles. Similar observations in smaller Au−Pd alloy nanoclusters (up to 55 atoms per cluster) have been reported by Pittaway and co-workers.[38] Adzic and co-workers reported a similar enhanced durability of PdAu@Pt particles.[33] Their study suggested that when a surface vacancy is formed in the Pt shell, Au is more likely to hop to the vacancy than Pd, which is another possible reason for inversion suppression. The important point is that trends in DFT-calculated CO binding energies using a partial-shell model correlate well with the koppa-shaped activity trend observed experimentally.

To conclude, we have reported an unusual koppa-shaped activity trend for adsorbed CO oxidation using $Pd_xAu_{140-x}$@Pt DEN electrocatalysts. Both experiments and DFT calculations suggest that this unusual behavior is caused primarily by structural changes of the DENs at high and low values of $x$. That is, a pure Au core leads to deformation of the Pt shell and a compression of the Pt lattice. However, Pd, from the pure Pd cores, tends to segregate on the DEN surface forming an inverted configuration having Pt within the core and Pd in the shell. In contrast, the alloy PdAu cores stabilize the core@shell structures by preventing Au and Pd from escaping the core. These findings illustrate the importance of controlling both the stability and reactivity of the catalysts, and they provide guidance as to how core composition can be used to do that. Above all, however, this study illustrates that nanoparticle structure, not just electronic effects, is a critically important factor for nanoscale electrocatalysts.

## ■ ASSOCIATED CONTENT

### Supporting Information

Experimental methods; computational methods; CVs of $Pd_xAu_{140-x}$ and $Pd_xAu_{140-x}$@Pt DENs in 0.1 M $HClO_4$; CVs of Cu UPD on $Pd_xAu_{140-x}$ DENs; $V_{l,OCP}$ for different $Pd_xAu_{140-x}$ cores; quantitative analysis of the galvanic exchange of the Cu shell for Pt; additional TEM images of $Pd_{70}Au_{70}$ and $Pd_{70}Au_{70}$@Pt, $Pt_{140}$, and $Pt_{140}$@Pd DENs; CO stripping voltammograms for $Pd_xAu_{140-x}$@Pt, $Pt_{140}$, $Pd_{140}$, and $Au_{140}$ DENs; CVs of $Pd_xAu_{140-x}$@Pt DENs in 0.10 M $HClO_4$ before and after CO stripping experiments; charge associated with the CO oxidation peaks versus that of the corresponding H adsorption wave areas for $Pd_xAu_{140-x}$@Pt DENs; OH binding energy; calculated average Pt−Pt bond lengths for $Pd_xAu_{140-x}$@Pt DENs; formation energy convex hull of PdAu alloy nanoparticles. The Supporting Information is available free of charge on the ACS Publications website at DOI: 10.1021/acs.jpclett.5b00985.

## ■ AUTHOR INFORMATION


### Corresponding Authors

*E-mail: henkelman@cm.utexas.edu.
*E-mail: crooks@cm.utexas.edu.

### Author Contributions

‖(L.L., L.Z.) These authors contributed equally.


### Notes

The authors declare no competing financial interest.

## ■ ACKNOWLEDGMENTS

We gratefully acknowledge support from the Chemical Sciences, Geosciences, and Biosciences Division, Office of Basic Energy Sciences, Office of Science, U.S. Department of Energy (Contract: DE-FG02-13ER16428). R.M.C. and G.H. thank the Robert A. Welch Foundation (Grants F-0032 and F-1841, respectively) for sustained support. This work was also supported, in part, by the National Research Foundation of Korea funded by the Ministry of Science, ICT and Future Planning (grant #: NRF-2014S1A2A2028540).

## ■ REFERENCES


(1) Studt, F.; Sharafutdinov, I.; Abild-Pedersen, F.; Elkjær, C. F.; Hummelshøj, J. S.; Dahl, S.; Chorkendorff, I.; Nørskov, J. K. Discovery of a Ni−Ga Catalyst for Carbon Dioxide Reduction to Methanol. *Nat. Chem.* **2014**, *6*, 320−324.

(2) Zhang, L.; Henkelman, G. Tuning the Oxygen Reduction Activity of Pd Shell Nanoparticles with Random Alloy Cores. *J. Phys. Chem. C* **2012**, *116*, 20860−20865.

(3) Zhang, L.; Iyyamperumal, R.; Yancey, D. F.; Crooks, R. M.; Henkelman, G. Design of Pt-Shell Nanoparticles with Alloy Cores for the Oxygen Reduction Reaction. *ACS Nano* **2013**, *7*, 9168−9172.

(4) Falsig, H.; Hvolbæk, B.; Kristensen, I. S.; Jiang, T.; Bligaard, T.; Christensen, C. H.; Nørskov, J. K. Trends in the Catalytic CO Oxidation Activity of Nanoparticles. *Angew. Chem., Int. Ed.* **2008**, *47*, 4835−4839.

(5) Nørskov, J. K.; Bligaard, T.; Rossmeisl, J.; Christensen, C. H. Towards the Computational Design of Solid Catalysts. *Nat. Chem.* **2009**, *1*, 37−46.

(6) Stamenkovic, V. R.; Mun, B. S.; Arenz, M.; Mayrhofer, K. J. J.; Lucas, C. A.; Wang, G.; Ross, P. N.; Markovic, N. M. Trends in Electrocatalysis on Extended and Nanoscale Pt−Bimetallic Alloy Surfaces. *Nat. Mater.* **2007**, *6*, 241−247.

(7) Zhang, L.; Henkelman, G. Computational Design of Alloy−Core@Shell Metal Nanoparticle Catalysts. *ACS Catal.* **2015**, *5*, 655−660.

(8) Cheng, D.; Xu, H.; Fortunelli, A. Tuning the Catalytic Activity of Au−Pd Nanoalloys in CO Oxidation via Composition. *J. Catal.* **2014**, *314*, 47−55.

(9) Su, R.; Tiruvalam, R.; Logsdail, A. J.; He, Q.; Downing, C. A.; Jensen, M. T.; Dimitratos, N.; Kesavan, L.; Wells, P. P.; Bechstein, R.; et al. Designer Titania-Supported Au−Pd Nanoparticles for Efficient Photocatalytic Hydrogen Production. *ACS Nano* **2014**, *8*, 3490−3497.

(10) Yancey, D. F.; Carino, E. V.; Crooks, R. M. Electrochemical Synthesis and Electrocatalytic Properties of Au@Pt Dendrimer-




DOI: 10.1021/acs.jpclett.5b00985
J. Phys. Chem. Lett. 2015, 6, 2562−2568

Encapsulated Nanoparticles. *J. Am. Chem. Soc.* **2010**, *132*, 10988−10989.
(11) Yancey, D. F.; Zhang, L.; Crooks, R. M.; Henkelman, G. Au@Pt Dendrimer Encapsulated Nanoparticles as Model Electrocatalysts for Comparison of Experiment and Theory. *Chem. Sci.* **2012**, *3*, 1033−1040.
(12) Iyyamperumal, R.; Zhang, L.; Henkelman, G.; Crooks, R. M. Efficient Electrocatalytic Oxidation of Formic Acid Using Au@Pt Dendrimer-Encapsulated Nanoparticles. *J. Am. Chem. Soc.* **2013**, *135*, 5521−5524.
(13) Carino, E. V.; Crooks, R. M. Characterization of Pt@Cu Core@Shell Dendrimer-Encapsulated Nanoparticles Synthesized by Cu Underpotential Deposition. *Langmuir* **2011**, *27*, 4227−4235.
(14) Carino, E. V.; Kim, H. Y.; Henkelman, G.; Crooks, R. M. Site-Selective Cu Deposition on Pt Dendrimer-Encapsulated Nanoparticles: Correlation of Theory and Experiment. *J. Am. Chem. Soc.* **2012**, *134*, 4153−4162.
(15) Maroun, F.; Ozanam, F.; Magnussen, O. M.; Behm, R. J. The Role of Atomic Ensembles in the Reactivity of Bimetallic Electrocatalysts. *Science* **2001**, *293*, 1811−1814.
(16) Knecht, M. R.; Weir, M. G.; Frenkel, A. I.; Crooks, R. M. Structural Rearrangement of Bimetallic Alloy PdAu Nanoparticles within Dendrimer Templates to Yield Core/Shell Configurations. *Chem. Mater.* **2007**, *20*, 1019−1028.
(17) Weir, M. G.; Knecht, M. R.; Frenkel, A. I.; Crooks, R. M. Structural Analysis of PdAu Dendrimer-Encapsulated Bimetallic Nanoparticles. *Langmuir* **2009**, *26*, 1137−1146.
(18) Zhou, H.; Park, J. H.; Fan, F.-R. F.; Bard, A. J. Observation of Single Metal Nanoparticle Collisions by Open Circuit (Mixed) Potential Changes at an Ultramicroelectrode. *J. Am. Chem. Soc.* **2012**, *134*, 13212−13215.
(19) Park, J. H.; Zhou, H.; Percival, S. J.; Zhang, B.; Fan, F.-R. F.; Bard, A. J. Open Circuit (Mixed) Potential Changes Upon Contact between Different Inert Electrodes−Size and Kinetic Effects. *Anal. Chem.* **2012**, *85*, 964−970.
(20) Leff, D. V.; Ohara, P. C.; Heath, J. R.; Gelbart, W. M. Thermodynamic Control of Gold Nanocrystal Size: Experiment and Theory. *J. Phys. Chem.* **1995**, *99*, 7036−7041.
(21) Maillard, F.; Eikerling, M.; Cherstiouk, O. V.; Schreier, S.; Savinova, E.; Stimming, U. Size Effects on Reactivity of Pt Nanoparticles in CO Monolayer Oxidation: The Role of Surface Mobility. *Faraday Discuss.* **2004**, *125*, 357−377.
(22) Chen, G.; Liao, M.; Yu, B.; Li, Y.; Wang, D.; You, G.; Zhong, C.-J.; Chen, B. H. Pt Decorated PdAu/C Nanocatalysts with Ultralow Pt Loading for Formic Acid Electrooxidation. *Int. J. Hydrogen Energy* **2012**, *37*, 9959−9966.
(23) Hofstead-Duffy, A. M.; Chen, D.-J.; Sun, S.-G.; Tong, Y. J. Origin of the Current Peak of Negative Scan in the Cyclic Voltammetry of Methanol Electro-Oxidation on Pt-Based Electrocatalysts: A Revisit to the Current Ratio Criterion. *J. Mater. Chem.* **2012**, *22*, 5205−5208.
(24) Babu, P. K.; Kim, H. S.; Chung, J. H.; Oldfield, E.; Wieckowski, A. Bonding and Motional Aspects of CO Adsorbed on the Surface of Pt Nanoparticles Decorated with Pd. *J. Phys. Chem. B* **2004**, *108*, 20228−20232.
(25) Zhou, W. P.; Lewera, A.; Larsen, R.; Masel, R. I.; Bagus, P. S.; Wieckowski, A. Size Effects in Electronic and Catalytic Properties of Unsupported Palladium Nanoparticles in Electrooxidation of Formic Acid. *J. Phys. Chem. B* **2006**, *110*, 13393−13398.
(26) Goto, S.; Hosoi, S.; Arai, R.; Tanaka, S.; Umeda, M.; Yoshimoto, M.; Kudo, Y. Particle-Size- and Ru-Core-Induced Surface Electronic States of Ru-Core/Pt-Shell Electrocatalyst Nanoparticles. *J. Phys. Chem. C* **2014**, *118*, 2634−2640.
(27) Lee, S. W.; Chen, S.; Sheng, W.; Yabuuchi, N.; Kim, Y.-T.; Mitani, T.; Vescovo, E.; Shao-Horn, Y. Roles of Surface Steps on Pt Nanoparticles in Electro-oxidation of Carbon Monoxide and Methanol. *J. Am. Chem. Soc.* **2009**, *131*, 15669−15677.
(28) Arenz, M.; Mayrhofer, K. J. J.; Stamenkovic, V.; Blizanac, B. B.; Tomoyuki, T.; Ross, P. N.; Markovic, N. M. The Effect of the Particle Size on the Kinetics of CO Electrooxidation on High Surface Area Pt Catalysts. *J. Am. Chem. Soc.* **2005**, *127*, 6819−6829.
(29) Park, S.; Xie, Y.; Weaver, M. J. Electrocatalytic Pathways on Carbon-Supported Platinum Nanoparticles: Comparison of Particle-Size-Dependent Rates of Methanol, Formic Acid, and Formaldehyde Electrooxidation. *Langmuir* **2002**, *18*, 5792−5798.
(30) Maillard, F.; Schreier, S.; Hanzlik, M.; Savinova, E. R.; Weinkauf, S.; Stimming, U. Influence of Particle Agglomeration on the Catalytic Activity of Carbon-Supported Pt Nanoparticles in CO Monolayer Oxidation. *Phys. Chem. Chem. Phys.* **2005**, *7*, 385−393.
(31) Anderson, R. M.; Zhang, L.; Loussaert, J. A.; Frenkel, A. I.; Henkelman, G.; Crooks, R. M. An Experimental and Theoretical Investigation of the Inversion of Pd@Pt Core@Shell Dendrimer-Encapsulated Nanoparticles. *ACS Nano* **2013**, *7*, 9345−9353.
(32) Koenigsmann, C.; Sutter, E.; Adzic, R. R.; Wong, S. S. Size- and Composition-Dependent Enhancement of Electrocatalytic Oxygen Reduction Performance in Ultrathin Palladium−Gold ($Pd_{1-x}Au_x$) Nanowires. *J. Phys. Chem. C* **2012**, *116*, 15297−15306.
(33) Sasaki, K.; Naohara, H.; Choi, Y.; Cai, Y.; Chen, W.-F.; Liu, P.; Adzic, R. R. Highly Stable Pt Monolayer on PdAu Nanoparticle Electrocatalysts for the Oxygen Reduction Reaction. *Nat. Commun.* **2012**, *3*, 1115.
(34) Gilman, S. A Study of the Mechanism of Carbon Monoxide Adsorption on Platinum by a New Electrochemical Procedure. *J. Phys. Chem.* **1963**, *67*, 78−84.
(35) Bandarenka, A. S.; Varela, A. S.; Karamad, M.; Calle-Vallejo, F.; Bech, L.; Perez-Alonso, F. J.; Rossmeisl, J.; Stephens, I. E. L.; Chorkendorff, I. Design of an Active Site Towards Optimal Electrocatalysis: Overlayers, Surface Alloys and Near-Surface Alloys of Cu/Pt(111). *Angew. Chem.* **2012**, *124*, 12015−12018.
(36) Strasser, P.; Koh, S.; Anniyev, T.; Greeley, J.; More, K.; Yu, C.; Liu, Z.; Kaya, S.; Nordlund, D.; Ogasawara, H.; et al. Lattice-Strain Control of the Activity in Dealloyed Core−Shell Fuel Cell Catalysts. *Nat. Chem.* **2010**, *2*, 454−460.
(37) Adzic, R. R.; Zhang, J.; Sasaki, K.; Vukmirovic, M. B.; Shao, M.; Wang, J. X.; Nilekar, A. U.; Mavrikakis, M.; Valerio, J. A.; Uribe, F. Platinum Monolayer Fuel Cell Electrocatalysts. *Top. Catal.* **2007**, *46*, 249−262.
(38) Pittaway, F.; Paz-Borbón, L. O.; Johnston, R. L.; Arslan, H.; Ferrando, R.; Mottet, C.; Barcaro, G.; Fortunelli, A. Theoretical Studies of Palladium-Gold Nanoclusters: Pd−Au Clusters with up to 50 Atoms. *J. Phys. Chem. C* **2009**, *113*, 9141−9152.


DOI: 10.1021/acs.jpclett.5b00985
*J. Phys. Chem. Lett.* 2015, 6, 2562−2568